Prabha Materials Science Letters
Vol. 5, No. 2, 258-271, 2026
https://doi.org/10.33889/PMSL.2026.5.2.014

Bio-synthesis of Silver Nanoparticles using Rhododendron Arboreum and their Role in Anionic Dye Degradation

Chetan Pant
Department of Physics,
Govind Ballabh Pant University of Agriculture & Technology, 263145, Pantnagar, Uttarakhand, India.
E-mail: chetanpant.1434@gmail.com

Divyanshu Pant
Department of Physics,
Govind Ballabh Pant University of Agriculture & Technology, 263145, Pantnagar, Uttarakhand, India.
E-mail: divyanshupant01@gmail.com

Puja Goel
Department of Physics,
Govind Ballabh Pant University of Agriculture & Technology, 263145, Pantnagar, Uttarakhand, India.
Corresponding author: pujagoel.bpp@gbpuat.ac.in, pujagoel@gmail.com

(Received on October 28, 2025; Revised on January 13, 2026 & March 1, 2026 & March 22, 2026 & March 31, 2026 & April 9, 2026; Accepted on April 10, 2026)

Abstract
In this study, the green synthesis of silver nanoparticles (AgNPs) using leaf extract from *Rhododendron arboreum* and a silver salt was investigated. pH of the solution was adjusted to 7, 8, 9, and 10 to examine the effects of neutral and alkaline conditions on the size, polydispersity, and stability of the synthesized AgNPs and their influence on the removal efficiency of the anionic methyl orange dye. FTIR analysis revealed the presence of phytochemicals in the leaf extract and their role in reducing Ag^+ ions from $AgNO_3$ to form AgNPs. The as-synthesized AgNP nano-suspension was directly employed for the dye degradation study. Dye degradation efficiency of AgNPs was evaluated using UV-visible absorption spectra, showing the highest efficiency (88%) at pH-8, significantly higher than at pH-7 (43%), and at pH-9 and 10, where the efficiencies were 78% and 70%, respectively. These results indicate that alkaline pH enhances the hydroxyl radical generation, which facilitates dye degradation. However, the efficiency is also affected by the properties of nanoparticles, such as size and polydispersity index (PDI), with the zeta potential playing a less significant role in this case. The optimal dye degradation efficiency was observed with AgNPs synthesized at pH-8, where there was a favourable balance between hydroxyl ion concentration and nanoparticle properties.

Keywords- AgNPs, UV-visible spectroscopy, Zeta potential, Dye degradation, Photodegradation.

1. Introduction

Nanotechnology has become a cornerstone of contemporary scientific progress, transforming how nanoparticles are created, engineered, studied, and applied. Across fields as diverse as medicine, drug delivery, optics, energy, optoelectronics, photo-electrochemical systems, and space exploration, these particles are pushing boundaries in ways that improve current technologies while laying the groundwork for tomorrow's breakthroughs. Silver nanoparticles (AgNPs) have gained a lot of research interest due to their exceptional antimicrobial, optical, and electrical properties among the most actively studied. These properties are affected by their shape and size. To produce AgNPs, researchers have explored many approaches, including chemical reduction, laser ablation, electron irradiation, photochemical processing, and biological synthesis methods. However, some of these methods have harmful effects on the environment and human health. To address these issues, biological synthesis, or green synthesis, is emerging as the more suitable alternative for producing and functionalizing nanoparticles since this

approach is biocompatible, eco-friendly, low in toxicity, and sustainable, rendering no hazardous waste behind (Bustos-Guadarrama et al., 2023; Gangwar & Joseph, 2025). By utilizing plant extracts, such as leaves, flowers, bark, and pollen, along with intracellular and extracellular enzymes and biodegradable polymers, we can obtain the necessary reducing and capping agents for the synthesis and stabilization of nanoparticles (Sharma et al., 2024). Several medicinal and non-medicinal plants, such as *Azadirachta indica* (Neem) (Babu et al., 2025), *Artocarpus heterophyllus* (Jackfruit) (Dewi et al., 2025), *Ocimum sanctum* (Tulsi) (Awasthi et al., 2025), and *Phyllostachys Aurea* (Bamboo) (Yasin et al., 2013), have been reported for the synthesis of AgNPs using leaf extracts. In line with this, leaves of the Himalayan plant *Rhododendron arboreum* (local name: Buransh) were chosen for the synthesis of Ag NPs for the current study, as the extracts from Rhododendron arboreum exhibit numerous biological activities, including anti-cancer, anti-diarrheal, anti-diabetic, anti-inflammatory, antioxidant, and antimicrobial properties (Rawat et al., 2017). Rhododendron arboreum is an evergreen tree with an average height of 45-50 feet, growing at elevations of 4500 to 10,500 feet, and is widely found in the hilly areas of Uttarakhand, Himachal Pradesh, Jammu & Kashmir, and other North-Indian states, as well as parts of Nepal. Tri-terpenoids and flavonoids are the phytochemicals that are mainly present in the leaves, act as reducing and capping agents, helping in stabilizing the nanoparticles. This study primarily investigates how pH conditions influence the synthesis of AgNPs and their subsequent efficiency in degrading the anionic dye, Methyl Orange.

The primary focus is on achieving controlled nanoparticle sizes for the purpose of wastewater remediation from dye contamination, as the wastewater from domestic and industrial activities often contains toxic components like dyes, pesticides, and hazardous chemicals, requiring effective removal methods to prevent harmful effects. Successful photocatalytic degradation of Chlorpyrifos pesticides using monodisperse gold nanoparticles for wastewater remediation is reported in previous research (Goel & Arora, 2020, Goel & Arora, 2022). Similarly, degradation of Methylene Blue dye was effectively done using silver nanopowder (Phuyal et al. 2022). However, large-scale synthesis and application of silver nanopowder can be costly. Gola et al. (2021) demonstrated the successful degradation of orange and blue dyes, both individually and in mixture, using sodium borohydride ($NaBH_4$). They also explored the use of chemically synthesized silver nanoparticles (AgNPs) combined with $NaBH_4$ as a catalyst, however, the specific role of the AgNPs in enhancing dye degradation efficiency remains unclear in their study. AgNPs immobilized on solid surfaces such as carbon nanotubes, amidoxime fibres, amorphous SiO_2, glass slides, and silica nanofibers are also effective in water remediation, particularly for dye removal (Zhou & Srinivasan, 2015). Immobilization improves the recyclability, recovery, and durability of AgNPs by facilitating their strong attachment to solid supports; however, the fabrication of such structures can be complex, and the catalytic efficiency of the nanoparticles often decreases due to limited access to the AgNPs embedded in the organic matrix. In view of these challenges, the current study aims to develop a simpler, more cost-effective, and environmentally friendly approach to dye degradation by synthesizing AgNPs through a green chemistry method. Aqueous leaf extract of *R. arboreum* (Buransh) was utilized to biosynthesize AgNPs. The reducing and capping agents present in the leaf extract, such as triterpenoids and flavonoids, facilitate the formation of AgNPs. The suspensions of biosynthesized AgNPs at varied pH values were directly introduced into a methyl orange dye solution. This method simplifies the process by ensuring that both the AgNPs and the dye are in the same phase, making it economically feasible and reducing the need for complex immobilization steps. The degradation efficiency against methyl orange was evaluated under varying conditions, including nanoparticle size, concentration, reaction time, and pH. The results were analyzed using UV-Visible spectrophotometry, FTIR spectroscopy, DLS and zeta potential analysis, providing insight into the degradation kinetics and the role of the AgNPs in the dye degradation process.

2. Materials and Methods

2.1 Materials

The fresh *Rhododendron arboreum* leaves were collected from Kunalta (29.7492°N, 79.8737°E), a distant village of Pithoragarh (Uttarakhand). Silver Nitrate ($AgNO_3$) was purchased from HiMedia Laboratories.

2.2 Preparation of Leaf Extract

20 g of fresh leaves were washed thoroughly with distilled water. After cutting into fine pieces, the leaves were boiled with 100 mL of distilled water in a 500 mL beaker at 620 °C for 30 minutes. The mixture was then cooled at room temperature for 40 minutes. It was filtered using Whatman no. 1 filter paper to prepare the leaf extract. The obtained leaf extract was stored at room temperature.

2.3 Synthesis of Nanoparticles

R. arboreum leaf extract was mixed with a 1 mM $AgNO_3$ solution in a 1:9 ratio and stirred at 500 rpm for 15 minutes at room temperature (33°C). The change in colour of the solution from pale to a yellowish-light brown indicates the successful synthesis of silver nanoparticles (AgNPs) (**Figure 1**). The colour was monitored in the intervals of 30 minutes, 60 minutes, and 24 hours. The colour of the solution reached a deep dark brown after 24 hours, and no colour change was observed after this point, indicating the complete reduction of the silver salt. The obtained AgNP sample was then stored in dark glass bottles wrapped in aluminium foil. The same process was repeated to synthesise AgNPs across a pH range of 5 to 10, adjusted using a 1 mM NaOH solution.

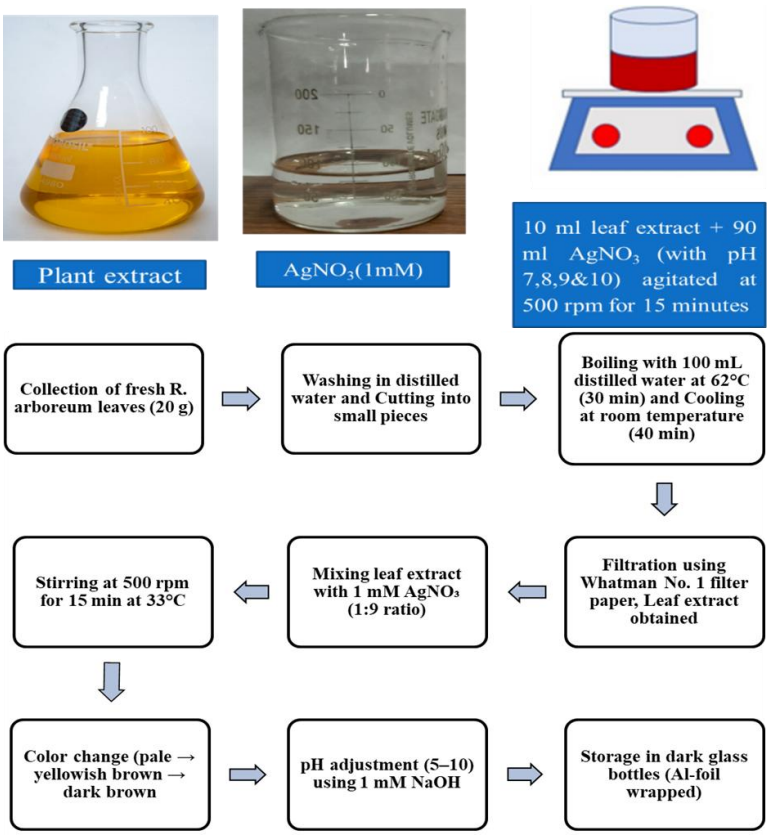

Figure 1. Synthesis of silver nanoparticles using *R. arboreum* leaf extract and $AgNO_3$.

2.4 Sample Preparation to Study Dye Removal Efficiency of Synthesized AgNPs

To prepare 20 ppm MO stock solution, 1 mg of MO (powdered form) was dissolved in 50 ml of DI water. From this solution, a 10 ppm concentration of MO was prepared. The sample batches were prepared by combining 5 ml of 10 ppm solution with AgNPs of varying sizes to investigate their effects. The reaction mixtures were exposed to sunlight for 5 hours, after which the extent of dye degradation was analysed using UV–vis spectrophotometer.

2.5 Characterization of AgNPs

The presence of the reducing and capping agents in leaf extract was investigated with the Attenuated Total Reflectance Fourier Transform infra-red (ATR-FTIR) spectroscopy, in the scanning range of 600 - 4000 cm^{-1} (Bruker Alpha FT-IR spectrometer). Optical absorption studies were done using *UV-Visible* spectrophotometer (Thermo Fisher Scientific G10S UV-Vis), in the scanning range of 200-600 nm. The average hydrodynamic radius of nanoparticles was measured with the help of the dynamic light scattering (DLS) method (Malvern Zetasizer Ver 7.11) and zeta potential measurements were carried out on Malvern Zetasizer Ver 2.3. The size and shape of the synthesized AgNPs was also confirmed by Transmission electron microscopy (TEM).

3. Results and Discussions

3.1 UV- vis Absorbance Analysis of Synthesized AgNPs

UV-vis spectroscopy measures the absorbance or transmittance in terms of surface plasmon resonance (SPR) in comparison to a reference sample. The absorbance generally depends on the time of reaction, temperature, pH of the sample, etc.

Figure 2. Colour of the AgNPs synthesized at pH-5 to pH-10.

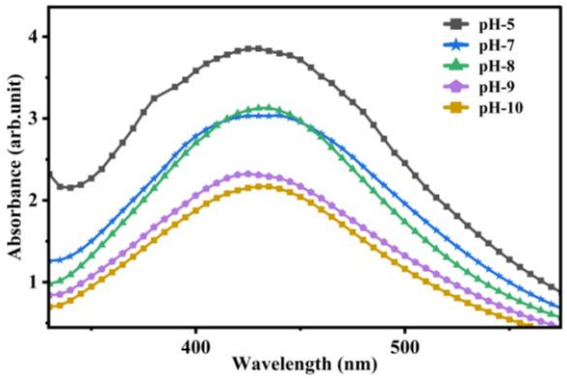

Figure 3. UV spectra of synthesized AgNPs at pH-5, pH-7, pH-8, pH-9 and pH-10.

In this study, a noticeable difference in the colour of the solution was observed with varying pH. At pH-5, the suspension appeared dark brown, gradually lightening as pH increased (**Figure 2**). The absorption maximum for pH-5 was observed at 425 nm (**Figure 3**). With increasing pH, the absorption maxima shifted to 435, 430, 420, and 435 nm for pH-7, 8, 9, and 10, respectively. Peak absorption intensity was observed at pH-8, indicating that this pH was most favourable for AgNP synthesis. However, with further increase in pH, the absorption intensity decreased, indicating the presence unstable and agglomerated nanoparticles (Tagad et al., 2013). These observations confirm that the highest yield of stable AgNPs occurred at pH 8.

3.2 Band Gap Energy Determination

The optical band gap energies of the biosynthesized AgNPs, determined from Tauc plots (**Figure 4(a–d)**) using the relation for a direct allowed transition $(\alpha h\nu)^2$ versus hν (Dhanya et al., 2020), showed a clear dependence on synthesis pH. The band gap energy of AgNPs corresponding to pH-7, 8, 9 and 10 with corresponding errors is summarised in **Table 1**. The band gap increased systematically from 3.90 eV at pH-7 to 4.08 eV at pH-10, indicating a widening of 0.18 eV across the studied pH range. Although particle size varied non-linearly with pH, the increase in band gap energy cannot be attributed to pH changes alone. Instead, multiple factors contribute to this behavior, with pH-induced agglomeration of AgNPs playing a key role (Zhou et al., 2016; Fernando & Zhou, 2019). Such agglomeration modifies interparticle interactions, surface states, and charge distribution, which collectively influence the optical response and electronic structure of the nanoparticles, leading to the observed variation in band gap energy.

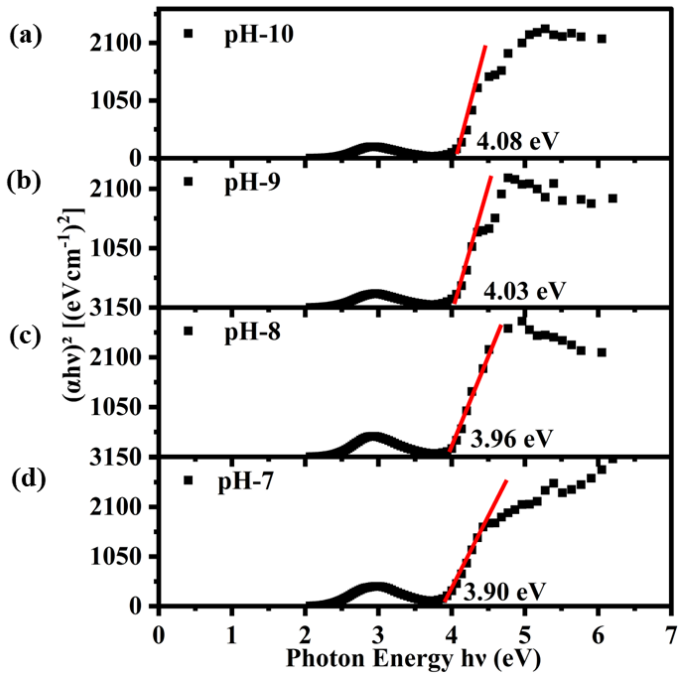

Figure 4. Tauc plot of AgNPs synthesized at (a) pH-7, (b) pH-8, (c) pH-9 and (d) pH-10.

3.3 ATR-FTIR Spectroscopy Analysis

The leaves of *Rhododendron arboreum* contain phenolic acids known for their anti-inflammatory, antioxidant, anti-HIV, and anti-nociceptive properties (Srivastava, 2012). The role of these phenolic acids as reducing agents for silver salts, as well as capping agents for the stabilization of nanoparticles, was

investigated using FTIR spectra. **Figure 5** shows the FTIR spectrum of the *R. arboreum* leaf extract and AgNPs synthesized using the *R. arboreum* leaf extract. FTIR spectrum of the *R. arboreum* leaf extract, revealing the presence of various phytochemical functional groups responsible for the bioreduction of AgNPs. A broad absorption band in the 3700–3000 cm^{-1} region is attributed to O–H stretching vibrations of hydroxyl groups present in phenols and alcohols (Lingegowda et al., 2012; Mary & Indira, 2017). The peak at 3020 cm^{-1} corresponds to aromatic C–H stretching, while the band at 2783 cm^{-1} is associated with aliphatic C–H stretching vibrations. The weak bands observed at 2373 cm^{-1} and 2183 cm^{-1} may arise from atmospheric CO_2 or combination bands and hence are interpreted cautiously. The peak at 1736 cm^{-1} is assigned to C=O stretching vibrations of carbonyl groups such as carboxylic acids or esters (Lingegowda et al., 2012), while the band at 1591 cm^{-1} corresponds to aromatic C=C stretching, confirming the presence of phenolic constituents (Mary & Indira, 2017). Further, the peak at 1346 cm^{-1} is attributed to C–O stretching or O–H bending vibrations, and the band at 1003 cm^{-1} corresponds to C–O stretching vibrations of phenolic and alcoholic groups (Mary & Indira, 2017). The peak at 893 cm^{-1} is assigned to out-of-plane bending of aromatic C–H bonds, indicating substituted aromatic rings. These observations confirm the presence of polyphenols and oxygenated biomolecules, which can act as reducing and stabilizing agents in nanoparticle synthesis.

FTIR spectrum of AgNPs synthesized using the *R. arboreum* leaf extract shows a broad absorption band in the 3500-3000 cm^{-1} region, including peaks at 3742 and 3320 cm^{-1}, is attributed to O–H stretching vibrations of phenolic and alcohol groups (Lingegowda et al., 2012), indicating their involvement in nanoparticle formation. Compared with the leaf extract, slight shifts and intensity changes suggest that these functional groups interact with the nanoparticle surface. The band at 2131 cm^{-1} is weak and may arise from overtone or combination bands and therefore, is interpreted cautiously. The peaks at 1748 cm^{-1} and 1638 cm^{-1} are assigned to C=O stretching of carbonyl groups and/or aromatic C=C vibrations (Dangi et al., 2020; Lingegowda et al., 2012), indicating the involvement of carbonyl and aromatic groups in nanoparticle formation. The band at 1372 cm^{-1} corresponds to C–O stretching or O–H bending vibrations. Peaks in the 1179-1045 cm^{-1} region are attributed to C–O stretching vibrations of phenolic compounds (Mary & Indira, 2017). The shifts in peak positions and changes in intensity compared to the leaf extract indicate the participation of these functional groups in both the reduction of Ag^{+} ions and the stabilization of the resulting AgNPs.

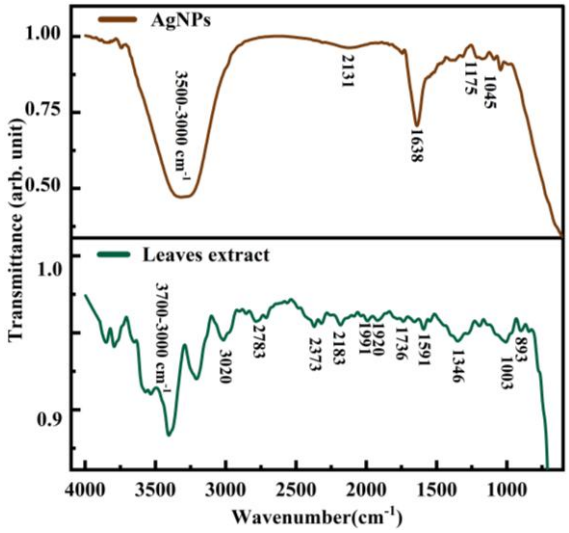

Figure 5. FTIR spectra of *R. arboreum* leaf extract and synthesized AgNPs.

3.4 Dynamic Light Scattering (DLS) and Zeta Potential Analysis

DLS and zeta potential analysis were used for the measurement of size (hydrodynamic) and surface charge of NPs, which are in emulsion or in liquid solution. Here, the particle size was calculated using the Stokes-Einstein formula, which is based on the fact that the diffusion coefficient is inversely proportional to the hydrodynamic diameter (d_p) of the particle (Bhattacharjee, 2016).

$$Diameter(d_p) = \frac{kT}{3\pi\eta D}.$$

where, k is the Boltzmann constant =1.38 x 10^{-23} kg-m^2-sec^{-2}-K^{-1}, T is the temperature, η is the viscosity of the liquid and D is the diffusion coefficient.

Figure 6 (a-d) presents the Dynamic Light Scattering (DLS) data of nanoparticles (NPs) synthesized at different pH values. At pH-7, the average hydrodynamic size of the AgNPs was approximately 55.07 nm, with a Polydispersity Index (PDI) of 0.556, indicating a relatively broad size distribution (**Figure 6(a)**). This suggests that the particle size distribution was non-uniform and varied across the sample.

At pH-8, the average particle size increased to around 71 nm, with a sharp peak observed at 77.71 nm (**Figure 6(b)**). This sharp peak suggests that approximately 99% of the particles are in this size range, while a small fraction of larger clusters (around 5.5 µm) was also present. The PDI value of 0.368 reflects a relatively good monodispersity, indicating that the particle sizes were more uniform than the pH-7 sample.

At pH-9, the average size of the nanoparticles further increased to approximately 90 nm, having a PDI value of 0.334 (**Figure 6(c)**). This indicates a more uniform dispersion compared to pH-7, with fewer size variations within the nanoparticle population. Interestingly, at pH-10, the average size of the nanoparticles decreased slightly to 66.81 nm, with a PDI of 0.376 (**Figure 6(d)**). This suggests that at pH-10, the nanoparticle suspension remained relatively monodisperse, despite the slight decrease in size.

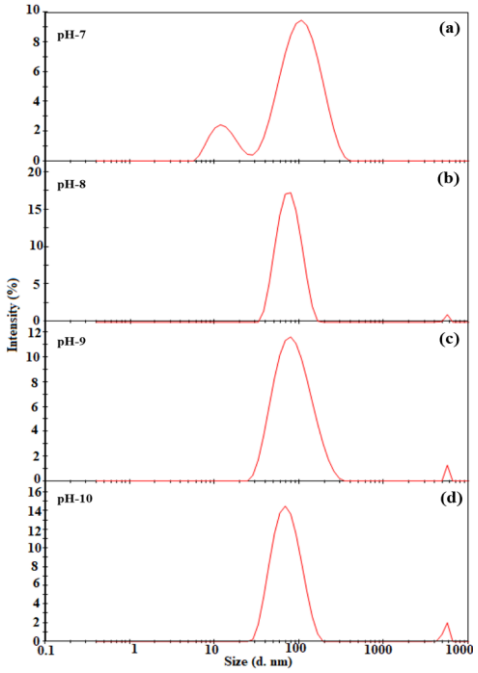

Figure 6. Size distribution of AgNPs synthesized at (a) pH 7, (b) pH 8 (c) pH 9 and (d) pH 10 using DLS.

Overall, these results suggest that the average size of the nanoparticles tended to increase with an increase in the pH of the nanosuspension up to pH-9. However, beyond pH-9, a reduction in particle size was observed. Moreover, the PDI of the nanoparticles exhibited an inverse relationship with the pH increase, decreasing as the pH rose from 7 to 9, which indicates improved uniformity and less variation in nanoparticle size. However, beyond pH-9, the trend reversed, with the PDI increasing despite the slight decrease in particle size. This observation may be attributed to changes in surface charge, stability, or aggregation behaviour at higher pH values. Typically, pH can affect the surface chemistry and charge distribution of nanoparticles, leading to aggregation or dispersion, which can be observed as changes in both the hydrodynamic size and PDI.

The zeta potential of AgNPs synthesized at different pH values was measured and is shown in **Figure 7**. The corresponding values of zeta potential for the different AgNPs are summarized in **Table 1**. At pH-7, the zeta potential was recorded as -11.3 mV, which increased to -16.7 mV at pH-8, the maximum value observed across all pH levels. Further increases in pH resulted in slightly less negative zeta potential values of -15.2 mV at pH-9 and -16.6 mV at pH-10. Negative zeta potential across which is pH-7 to pH-10 range indicates that particle surface acquires a negative surface charge with a positively charged stern layer around particle surface.

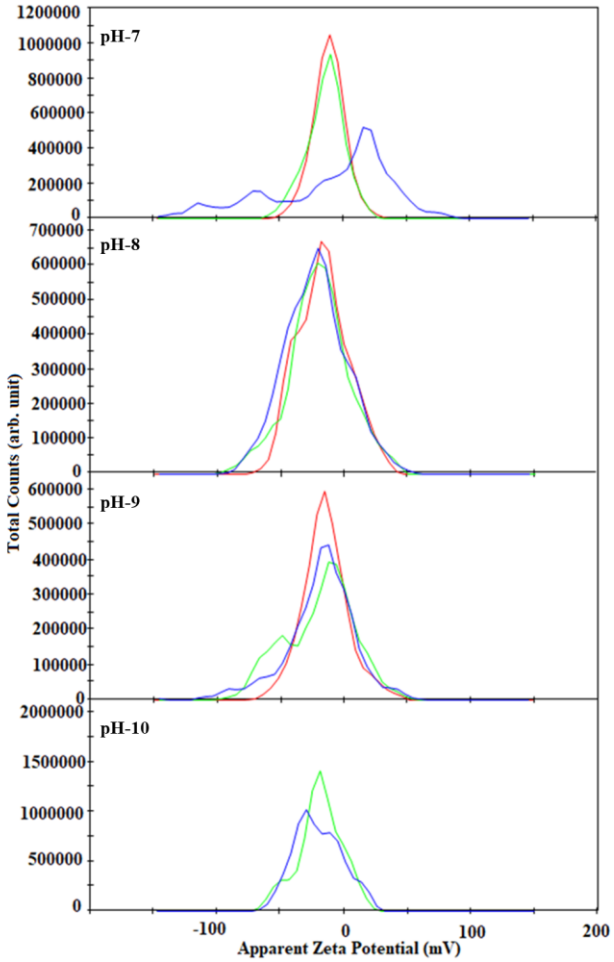

Figure 7. Zeta potential of AgNPs synthesized at pH-7, pH-8, pH-9 and pH-10.

3.5 Transmission Electron Microscopy (TEM) Analysis

The size and shape of AgNPs in nanosuspension having pH-8 was analyzed with TEM, as shown in **Figure 8**. TEM images confirmed that particles are in oval shape and have an average size of 32 nm.

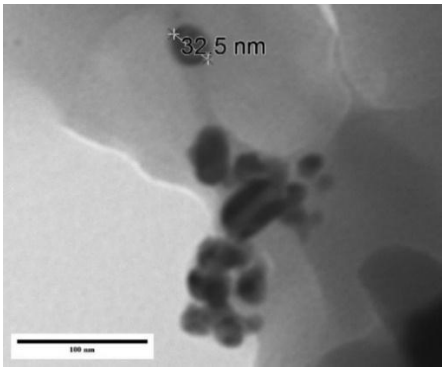

Figure 8. TEM images of AgNPs synthesized at pH-8 (100 nm scale).

3.6 Catalytic Activity of Synthesized Ag NPs in MO Dye Degradation

The catalytic activity of AgNPs in nano-suspension, with particles of varying sizes across a pH range of 7 to 10, was assessed by evaluating their efficiency in degrading Methyl Orange (MO) dye under sunlight exposure. Suspensions containing AgNPs at different pH levels were added to a 10 ppm MO solution and subjected to sunlight irradiation for 5 hours. A visible colour change in the solution (**Figure 9**) was observed, indicating the degradation of the MO dye by the AgNPs. Upon exposure to sunlight (hυ), Ag NPs generate electron-hole pairs ($Ag^0 + h\upsilon \rightarrow h^+$-VB + e^-). These electron-hole pairs can act as potent oxidizing agents (h^+-VB + $OH^- \rightarrow OH$) or reducing agents ($O_2 + e^- \rightarrow O_2^{\bullet-}$). In a hydroxyl-rich environment (pH-8 to 10), the holes generated on the AgNP surface facilitate the production of hydroxyl radicals (OH) through photo-oxidation (Agnihotri et al., 2018). These hydroxyl radicals play a pivotal role as the primary oxidizing species and are responsible for MO dye degradation, as they effectively attack the dye molecules, breaking their chromophore structure. The breakdown of the chromophore disrupts the dye's ability to absorb light, leading to reduced colour intensity of the dye solution. This oxidative degradation ultimately results in the decolorization and breakdown of the MO dye, rendering it less toxic or even non-toxic.

Quantitative assessment of degradation efficiency was done by utilizing the UV-visible absorption spectra of 10 ppm MO dye treated with AgNPs synthesized at different pH values, as presented in **Figure 10**. The removal efficiency was calculated using the following formula:

$$\% \text{ Removal} = \frac{A_1 - A_2}{A_1} \times 100.$$

where, A_1 and A_2 are the absorbances of the dye before and after treatment, respectively. **Table 1** summarizes the dye removal efficiency of AgNPs at different pH values, both before and after centrifugation. The removal efficiency at neutral pH (pH-7) for 10 ppm MO dye was approximately 43%. However, as the pH increased to 8, a significant improvement in efficiency was observed, reaching to a peak value of 88%, which was the highest removal efficiency across the pH range from 7 to 10. Further increases in pH to 9 and 10 led to a decline in efficiency, with values decreasing to approximately 78% and 70%, respectively. These results highlight the critical role of pH, while also suggesting that other factors, such as the size, polydispersity index (PDI), and zeta potential of the AgNPs, are crucial in optimizing dye removal.

An increase in pH typically elevates the concentration of hydroxyl ions (OH^-), which can exert a dual influence on the degradation process. Higher pH facilitates the generation of hydroxyl radicals (•OH) via photo-oxidation, promoting the breakdown of dye molecules, and the rise in pH can also increase the negative surface charge of the AgNPs, potentially causing electrostatic repulsion between the negatively charged AgNPs and the anionic MO dye molecules. This repulsive interaction can hinder effective contact between the AgNPs and the dye, thus reducing degradation efficiency. Interestingly, while the zeta potential of AgNPs synthesized at pH-8 was the most negative among the tested pH values, it still exhibited the highest degradation efficiency. This suggests that the enhanced generation of hydroxyl ions at pH 8 plays a more significant role in dye removal than the electrostatic repulsion between the particles and dye molecules. Alternatively, it can be said that the zeta potential did not seem to play an effective role across the samples studied. However, when the pH was raised further to 9 and 10, the decrease in efficiency to 78% and 70%, respectively, indicates that factors such as nanoparticle size and particle number become more influential at higher pH levels compared to the effect of hydroxyl radicals. Overall, the optimal dye removal efficiency in this study was achieved with AgNPs synthesized at pH-8, having an average hydrodynamic size of 71 nm, an optical band gap of 3.91 eV and a PDI of 0.368, where a balance between hydroxyl ion concentration and nanoparticle characteristics led to the most effective degradation of the dye.

Table 2 presents a comparative overview of previously reported photocatalysts for MO dye degradation with their corresponding degradation efficiencies. A careful examination of the table indicates that although some materials exhibit higher degradation efficiencies, such performance is often achieved under relatively high catalyst dosages, the use of chemical reductants, or irradiation sources other than natural sunlight. Hence, green-synthesized AgNPs in this study demonstrate efficient photocatalytic degradation of MO dye under irradiation of sunlight using a simple synthesis without any additional chemical agent or complex immobilization strategies. The optimal performance observed for AgNPs synthesized at pH-8 highlights the advantage of controlled synthesis conditions in achieving effective dye removal. These results demonstrate that the biosynthesized AgNPs hold significant potential as eco-friendly photocatalysts for wastewater treatment. Nevertheless, further studies are required to investigate their performance under a wider range of operating conditions, including variations in catalyst and dye concentration, pH of the solution, and long-term stability, to fully assess their applicability for practical water remediation.

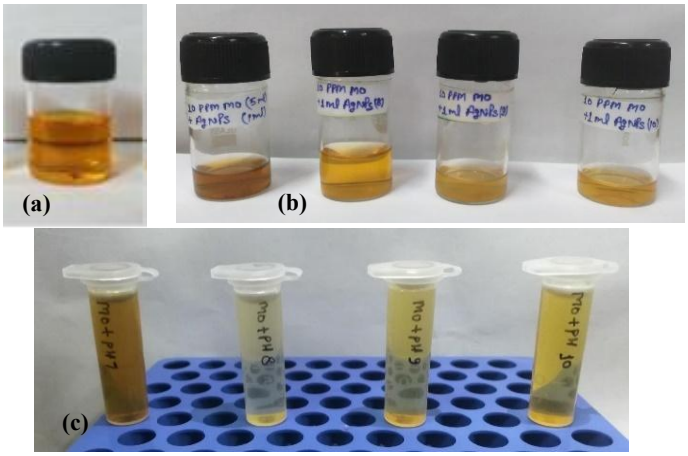

Figure 9. (a) Pure 10 ppm MO solution, (b) After degradation of samples using AgNPs of 7, 8, 9 and 10, respectively, (c) After centrifugation and decantation (acd).

Table 1. Dye degradation efficiency and band gap of AgNPs synthesized under different pH and having different sizes, PDI and Zeta potential.

pH of AgNPs	Band gap (eV)	Size (nm)	PDI	Zeta potential (mV)	% Dye removal (before)	% Dye removal (acd)
pH-7	3.90 ± 0.301	55.07	0.556	-11.3	38.65	43
pH-8	3.96 ± 0.399	71.17	0.368	-16.7	81.06	88
pH-9	4.03 ± 0.78	90	0.334	-15.2	64.97	78
pH -0	4.08 ± 0.66	66.81	0.376	-16.6	64.01	70

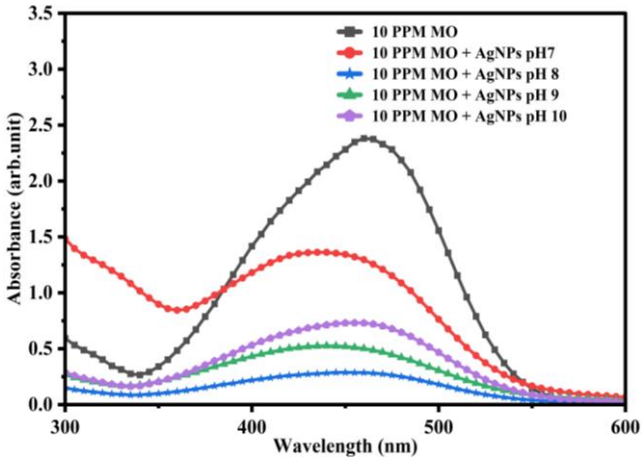

Figure 10. UV-Vis spectra of 10ppm MO dye treated by AgNPs synthesized at pH-7, pH-8, pH-9 and pH-10.

Table 2. Literature comparison of nanoparticle-based photocatalytic degradation of anionic dyes.

Material	Anionic dye	Dye concentration	Light condition	% Dye removal	Reference
AgNPs ($NaBH_4$-assisted)	MO	50 ppm	Ambient light	75	Gola et al. (2021)
AgNPs	MO	10 ppm	UV light	94	Zhou & Srinivasan (2015)
Gold nanoparticles	MO	200 ppm	Sun light	83.25% after 120 min.	Baruah et al. (2018)
ZnO nanoparticles	MO	10 ppm	UV light	87% after 120 min	Arroyo-Ortega et al. (2022)
Green synthesized AgNPs using *R. arboreum* leaf extract	MO	10 ppm	Sunlight irradiation	88 (at pH 8)	Present work

4. Conclusion

This work demonstrates a simple, green, and sustainable route for the synthesis of silver nanoparticles (AgNPs) using *Rhododendron arboreum* leaf extract and establishes their effective role in the sunlight-driven degradation of Methyl Orange (MO) dye. The synthesis process was sensitive to pH, which influenced nanoparticle formation, size distribution, and stability, as confirmed by UV–visible spectroscopy, DLS, TEM, and FTIR analyses. Among the investigated conditions, AgNPs synthesized at pH-8 exhibited optimal physicochemical characteristics, including a relatively uniform size distribution (average hydrodynamic size ~71 nm) and good dispersion, leading to the highest dye degradation efficiency of 88%. The degradation efficiency was significantly influenced by pH, with the highest removal observed at pH-8 (88%), where the generation of hydroxyl radicals played a key role in breaking down the dye molecules. Although the zeta potential of the AgNPs at pH-8 was the most negative, it was not the primary factor driving the dye degradation; instead, the enhanced hydroxyl ion concentration and favourable

nanoparticle characteristics at this pH were more critical. Overall, this study contributes meaningful insight toward the development of environmentally friendly AgNP-based photocatalysts for remediation applications. Future investigations will focus on designing cost-effective, scalable AgNP-based nanocomposites with improved stability and reusability, thereby strengthening their potential for practical and sustainable wastewater treatment.

Conflicts of Interest

The authors declare that they have no known competing financial interests or personal relationships that could have appeared to influence the work reported in this paper.

Acknowledgments

The authors sincerely thank the Vice-Chancellor of G.B.P.U.A.T., Pantnagar, for continuous encouragement and support. They also thank the Department of Chemistry, the Department of Environmental Sciences (EVS), and the Dean of C.B.S.H. for providing UV–Vis and FTIR facilities. The authors further thank Dr. Manika Khanuja, Jamia Millia Islamia, for assistance with zeta potential measurements.

AI Disclosure

During the preparation of this work the author(s) used generative AI in order to improve the language of the article. After using this tool/service, the author(s) reviewed and edited the content as needed and take(s) full responsibility for the content of the publication.

References

Agnihotri, S., Sillu, D., Sharma, G., & Arya, R.K. (2018). Photocatalytic and antibacterial potential of silver nanoparticles derived from pineapple waste: process optimization and modeling kinetics for dye removal. *Applied Nanoscience*, *8*(8), 2077-2092.

Arroyo-Ortega, G., Paz, J.F., Armendariz, I.O., Camacho-Montes, H., León, C., Reyes-Blas, H., & Rodríguez-González, C.A. (2022). Photocatalytical degradation of methyl orange (MO) using ZnO nanoparticles from alkaline wasted batteries. The effect of the MO, catalyst, and organic loads. *Digest Journal of Nanomaterials & Biostructures*,*17*(4), 1241-1248.

Awasthi, S., Sheeja, M.S., Chethana, V.C., & Shaji, L. (2025). Formulation of herbal anti-dandruff shampoo incorporating green synthesized silver nanoparticles from Tulsi Ocimum sanctum leaf extract. *VLEARNY Journal of Biological Sciences*, *1*(2), 10-17.

Babu, A.B., Rao, Y.S., Sravanthi, P., Miditana, S.R., Pulsingh, D., & Bhavani, A.D. (2025). Green synthesis of silver nanoparticles using Azadirachta indica (Neem) fruit pulp extract and their antioxidant, antibacterial, and anticancer activity. *Sustainable Chemistry for the Environment*, *11*, 100282. https://doi.org/10.1016/j.scenv.2025.100282

Baruah, D., Goswami, M., Yadav, R.N.S., Yadav, A., & Das, A.M. (2018). Biogenic synthesis of gold nanoparticles and their application in photocatalytic degradation of toxic dyes. *Journal of Photochemistry and Photobiology B: Biology*, *186*, 51-58.

Bhattacharjee, S. (2016). DLS and zeta potential–what they are and what they are not?. *Journal of Controlled Release*, *235*, 337-351.

Bustos-Guadarrama, S., Nieto-Maldonado, A., Flores-Lopez, L.Z., Espinoza-Gomez, H., & Alonso-Nunez, G. (2023). Photocatalytic degradation of azo dyes by ultra-small green synthesized silver nanoparticles. *Journal of the Taiwan Institute of Chemical Engineers*, *142*, 104663. https://doi.org/10.1016/j.jtice.2022.104663

Dangi, S., Gupta, A., Gupta, D.K., Singh, S., & Parajuli, N. (2020). Green synthesis of silver nanoparticles using aqueous root extract of Berberis asiatica and evaluation of their antibacterial activity. *Chemical Data Collections*, *28*, 100411. https://doi.org/10.1016/j.cdc.2020.100411

Dewi, F.R., Rohmatika, A.U., Jamil, A.K., Demircan, T., Idris, M.F., Litazkiyyah, L., Fahmi, M., Rosyidah, A.L., Hayati, A., & Sugiharto, S. (2025). Plant-based synthesis of gold and silver nanoparticles using Artocarpus heterophyllus aqueous leaf extract and its anticancer activities. *Narra J*, *5*(2), e1770.

Dhanya, I., Varghese, L.M., Reji, S., Nithish, S., & Chandran, S. (2020). Synthesis and characterization studies of silver nano particles using homoeo medicine (Gelsemium Sempervirens). In *AIP Conference Proceedings* (Vol. 2263, No. 1, p. 060002). AIP Publishing LLC. Kothamangalam, India.

Fernando, I., & Zhou, Y. (2019). Impact of pH on the stability, dissolution and aggregation kinetics of silver nanoparticles. *Chemosphere*, *216*, 297-305.

Gangwar, J., & Joseph, K.S. (2025). Eco-conscious photocatalytic degradation of organic textile dyes using green synthesized silver nanoparticles: a safe and green approach toward sustainability. *Biomass Conversion and Biorefinery*, *15*(17), 23989-24000.

Goel, P., & Arora, M. (2020). Mechanism of visible-light-driven photocatalytic degradation of endosulfan pesticide by gold nanoparticles. *Environmental Research Communications*, *2*(7), 075004. https://doi.org/10.1088/2515-7620/aba440.

Goel, P., & Arora, M. (2022). Nano-engineered gold particles for pesticide mineralization in contaminated water. In *Nano-biotechnology for Waste Water Treatment: Theory and Practices* (pp. 227-252). Springer International Publishing, Cham, Switzerland.

Gola, D., Bhatt, N., Bajpai, M., Singh, A., Arya, A., Chauhan, N., Srivastava, S.K., Tyagi, P.K., & Agrawal, Y. (2021). Silver nanoparticles for enhanced dye degradation. *Current Research in Green and Sustainable Chemistry*, *4*, 100132.

Lingegowda, D.C., Kumar, J.K., Prasad, A.D., Zarei, M., & Gopal, S. (2012). FTIR spectroscopic studies on cleome gynandra-Comparative analysis of functional group before and after extraction. *Romanian Journal of Biophysics*, *22*(3-4), 137-143.

Mary, S.J., & Indira, S. (2017). Phytochemical and FT-IR spectral analysis of Rhododendron arboreum Sm. ssp. nilagiricum (Zenker) Tagg. *Bioscience. Discovery*, *8*(1), 9-13.

Phuyal, S., Lamichhane, G., Gupta, A., Khadayat, K., Adhikari, A., Marahatha, R., Khadka, S., & Parajuli, N. (2022). Biosynthesis of silver nanoparticles from Rhododendron arboreum for metal sensing, antibacterial assessment, and photocatalytic degradation. *Journal of Nanomaterials*, *2022*(1), 2110636.

Rawat, P., Rai, N., Kumar, N., & Bachheti, R.K. (2017). Review on Rhododendron arboreum-a magical tree. *Oriental Pharmacy and Experimental Medicine*, *17*(4), 297-308.

Sharma, A., Sunny, S., Arulraj, J., & Hegde, G. (2024). Exploring the efficiency of green synthesized silver nanoparticles as photocatalysts for organic dye degradation: unveiling key insights. *Nano Express*, *5*(2), 022002.

Srivastava, P. (2012). Rhododendron arboreum: an overview. *Journal of Applied Pharmaceutical Science*, *2*(1),158-162.

Tagad, C.K., Dugasani, S.R., Aiyer, R., Park, S., Kulkarni, A., & Sabharwal, S. (2013). Green synthesis of silver nanoparticles and their application for the development of optical fiber based hydrogen peroxide sensor. *Sensors and Actuators B: Chemical*, *183*, 144-149.

Yasin, S., Liu, L., & Yao, J.M. (2013). Biosynthesis of silver nanoparticles by bamboo leaves extract and their antimicrobial activity. *Journal of Fiber Bioengineering and Informatics*, *6*(1), 77-84.

Zhou, R., & Srinivasan, M.P. (2015). Photocatalysis in a packed bed: degradation of organic dyes by immobilized silver nanoparticles. *Journal of Environmental Chemical Engineering*, *3*(2), 609-616.

Zhou, W., Liu, Y.L., Stallworth, A.M., Ye, C., & Lenhart, J.J. (2016). Effects of pH, electrolyte, humic acid, and light exposure on the long-term fate of silver nanoparticles. *Environmental Science & Technology*, *50*(22), 12214-12224.

Original content of this work is copyright © Ram Arti Publishers. Uses under the Creative Commons Attribution 4.0 International (CC BY 4.0) license at https://creativecommons.org/licenses/by/4.0/

Publisher's Note- Ram Arti Publishers remains neutral regarding jurisdictional claims in published maps and institutional affiliations.